PAPER Nr.: 12

AN ANALYTICAL MODEL OF UNSTEADY PROFILE AERODYNAMICS AND ITS APPLICATION TO A ROTOR SIMULATION PROGRAM

by

B. G. van der Wall

German Aerospace Research Establishment (DLR)
Institut for Flight Mechanics, Braunschweig, West-Germany

FIFTEENTH EUROPEAN ROTORCRAFT FORUM

SEPTEMBER 12 - 15, 1989 AMSTERDAM

An analytical Model of unsteady Profile Aerodynamics and its Application to a Rotor Simulation Program

by

B. G. van der Wall
German Aerospace Research Establishment (DLR)
Institut for Flight Mechanics, Braunschweig, West-Germany

Abstract

Rotor simulation programs for use in the field of helicopter flight mechanics and even for studies in the field of higher harmonic control often are working with steady profile aerodynamics, calculating blade loadings by table look-up method with respect to local mach number and angle of attack. They are neglecting the phase differences between the geometrical and effective angle of attack (circulation lag effect) and the dynamic stall effects are represented by corrected lift coefficients at lower mach numbers only. In most cases sweep effects are not considered, too.

In this study an analytical mathematical model is used for description of steady and unsteady aerodynamic forces and moments of a profile including sweep effects. It is a modified version of the model of Mr. Leiss, who has presented it at several earlier European Rotorcraft Forums; here it is used with a set of parameters representing the aerodynamic coefficients of the NACA 23012 profile.

This aerodynamic model is implemented into a rotor simulation program describing the hingeless BO 105 model rotor of the DLR. All degrees of freedom are included in the form of uncoupled modal description in flap, lag and torsion. Two downwash models with respect to higher harmonic downwash components are investigated: the model of Mangler up to the 6th harmonic and a simple prescribed distorted wake geometry of Beddoes in a modified version.

The results of calculations in the range of $\mu = 0.0$ to $\mu = 0.35$ with a thrust coefficient of $C_T = 0.0056$ are presented indicating significant effects resulting from unsteady aerodynamics.

1 Introduction

Several wind tunnel tests have shown that the classical description of rotor simulation programs with rigid blades and an effective hinge, simple downwash models and table look-up method for calculating aerodynamic coefficients are usable for calculation of rotor performance but not sufficient enough to predict the level of vibratory loads. Nevertheless such models are used even for calculations with respect to higher harmonic control [1]. On the other hand the combination of higher order methods like Euler codes for aerodynamics [2] and Finite Element Methods for the elastomechanic behaviour are indiscussible for use in flight mechanics because of their enormous need of calculation time and memory.

To fill this deficiency several methods have been developed, representing unsteady lift and moment hysteresis [3], [4], [5] but most of them are limited to small angles of attack and are containing a lot of switches concerning the actual angle of attack α, the time derivative $\dot{\alpha}$ and mach number. The sweep effect is not represented.

However, in fast forward flight all angles of attack can occur at the retreating side including great sweep angles and therefore they have to be represented in simulation as well as higher order elastic behaviour of the blades and the wake has to be modelled including blade/vortex interaction effects, too. To fulfill all these requirements in a not too calculation time expansive way a compromise has been used in the following form:

1. Aerodynamics:
   An analytical method [6] represents the steady and unsteady aerodynamic coefficients even under sweep conditions without any switches.

2. Elastomechanic behaviour:
   Flapwise, lagwise and torsional bending of the blades are described by their uncoupled modal forms.

3. Downwash:
   Two downwash models are under consideration: Firstly, the method of Mangler [7] which gives downwash components of higher harmonic order; here used up to the 6th harmonic. Secondly, a distorted prescribed vortex geometry is used, following Beddoes [8].

By this way all important effects of unsteady airstream, unsteady aerodynamic coefficients and blade motion of higher order are under consideration without treating the calculation time more than absolutely necessary.

In this paper the main subject will be the combination of all those models with special emphasis to the implementation of the unsteady aerodynamic model and therefore the description of the parts concerning blade elastics and downwash is only short.

2 Rotor simulation program components

2.1 Blade elastics

The model rotor of the DLR is a mach-scaled version without precone of the hingeless BO105 rotor with a scaling factor of 2.5. For a better representation of Reynoldsnumber profile chord is reduced by a factor of only 2.23. The modes of the model rotor in flap, lag and torsion are known from a Finite Element calculation and for a better handling these modes Φ here are described by a 6th order polynom in the radial coordinate x

$$\Phi_j(x) = \sum_{l=1}^{6} a_{lj} \cdot x^l \qquad (Mode\ j)$$

With respect to the hingeless rotor the gradient at the blade root must be zero and therefore the coefficient a_{1j} vanishes. Fig. 1 shows the so identified modes for flapping, lagging and torsion of the DLR BO105 model rotor blades.

The amplitude of each point of the elastic blade axis is then given by multiplication with the generalized coordinate $q_j(t)$ and the blade length l_{Bl}. So vertical displacement z is represented by superposition of N_z flapping modes; lagging displacement y is formulated in the same way. Both are multiplied with the blade length l_{Bl} as the dimensioning factor and elastic torsion only has the multiplication factor of 1 because its dimension is radian.

$$z(x,t) = l_{Bl} \cdot \sum_{j=1}^{N_z} \Phi_{zj}(x) \cdot q_{zj}(t) \qquad y(x,t) = l_{Bl} \cdot \sum_{j=1}^{N_y} \Phi_{yj}(x) \cdot q_{yj}(t) \qquad \vartheta_{el}(x,t) = \sum_{j=1}^{N_\vartheta} \Phi_{\vartheta j}(x) \cdot q_{\vartheta j}(t)$$

Mass distribution is stepwise constant or linear and so all integrals concerning mass moments and mass forces can be calculated analytically before simulation starts. A coupling exists between flapping and lagging by Coriolis forces and so the differential equation for lagging is directly influenced by flapping motion.

The differential equation of torsional motion also contains an additional term resulting from the control settings of the rotor (mono and higher harmonic) which are acting as an exciter.

2.2 Downwash Modelling

2.2.1 The Method of Mangler

In helicopter simulation programs often a constant or trapezoidal downwash distribution is used. Because the 1st harmonic represents the only harmonic, this cannot be a useful way to predict rotor vibrations. On the other hand, free wake programs, even very modern ones like that from Bliss, Teske and Quakenbush [9] need too much calculation time. So it should be a good compromise using a higher order downwash model, that contains harmonic components up to several harmonics and such one is the Method of Mangler [7]. The results of his calculations are presented by a Fourier series [10] and therefore this method has two significant advantages:

- coefficients can be calculated before simulation starts
- non-uniform downwash distribution up to several harmonics without expanding calculation time is represented

The evaluation of the induced velocity (normal component) V_i is simple

$$V_i(r,t) = V_{i0}(C_T) \cdot \left[C_0(r) + \sum_{n=1}^{N_{har}} C_{nr}(r) \cdot C_{n\alpha}(\alpha_{Ro}) \cdot \cos(n \cdot \psi) \right]$$

For odd values of $n > 3$: $C_{nr} = 0$; V_{i0} represents the mean induced velocity as a function of thrust coefficient C_T following the Glauert formula. In this study the maximum number of harmonics considered is $N_{har} = 6$, because the values of $C_{n\alpha}$, $n > 6$ are decreasing to zero and the resonance frequencies of the blade elastic modes considered are below the 6th harmonic of the rotor. Moreover, the angle between the velocity normal and tangential to the rotor disc is used instead of the shaft angle α_{Ro}, following Johnson [11]. The effect of this are higher values in the coefficients $C_{n\alpha}$ at low speeds.

An example of the downwash distribution with this model is shown in Fig. 2 where positiv values indicate downwash. Basic data are an advance ratio of $\mu = 0.15$ and a thrust coefficient of $C_T = 0.0056$.

2.2.2 Prescribed Wake Method

A second wake model was used following Beddoes [8] in principle. The reason for this step was the fact that the method of Mangler is not able to represent special vortex effects like BVI and therefore it can describe the principal distribution of downwash only. The method of Beddoes is used here in a modified version where geometry of the distorted spiral is taken from Beddoes but every spiral is not replaced by two single straight vortices like he has proposed. At every azimuth of the future simulation calculation the following procedure is done:

1. Vortex element circulation is set to the value 1
2. The induced velocity component normal to the rotor disc of any vortex element is calculated by the Biot-Savart law, corrected in the vicinity of the vortex by the method of Scully [12]. This gives a set of influence coefficients from any vortex element to the points of interest inside the rotor disc
3. To every radial station considered the influence matrix of all vortex elements is calculated

By this way, a set of influence matrices can be precalculated and inside the simulation the evaluation of the local downwash reduces to the multiplication of a column of this matrix with the vector of calculated blade circulation of the last turn. This is a very fast method inside the simulation but the calculation of the influence matrices takes a lot of time, of course. Additionally this method is restricted to a special set of basic data and in principle there are no great changes allowed inside the simulation with respect to shaft angle and in thrust or moments of the rotor. Nevertheless, the model is used for calculation of dynamic loads of steady rotor condition and therefore these limitations are not affected.

In Fig. 3 an example for the distorted spiral geometry is given with the same basic data as in Fig. 2. It is to be seen that the path of tip vortices in the middle of the rotor moves faster downwards than at the sides where the vortices are only slowly moving down. This represents the vortex roll-up in principle. In Fig. 4 the downwash distribution in the rotor plane is given for the case of vortex geometry shown above. Here we can see that the Mangler method gives the mean distribution of downwash in a very good way and the vortex spiral method additionally represents discrete vortex effects as expected.

2.3 Calculation of aerodynamic coefficients

For description of the aerodynamic coefficients of the profile in lift, drag and moment a completely new way is used in the steady and unsteady case. The reason for this is the impossibility to get logical unsteady lift, drag or moment hysteresis loops out of table look-up methods. Here Leiss [6] has developed a very promising method: by analytical functions, whose parameters have to be identified by steady profile measurements, the steady behaviour in all coefficients is perfectly represented. Of course this set of parameters is relatively extensive (about 30 parameters for each coefficient), but every parameter has a physical meaning. This becomes very important when steady sweep is implemented [13] because only some parameters are affected by sweep and an analytic formulation of steady coefficients under sweep is given with only 2 additional parameters for every coefficient.

The main reason why Leiss developed this method was not the steady case but the possibility to calculate unsteady lift hysteresis loops with only a set of again 2 additional parameters as shown in [14] where he presented a set of 150 hysteresis loops for different mach numbers and a wide spectrum of reduced frequencies. Agreement with measurements is much better than other methods can do (like those of Gormont or Gangwani) as he has shown. This has been the reason for us to use this analytical method for representation of unsteady coefficients in a rotor simulation program.

2.3.1 Steady aerodynamic coefficients

In the following the method is described only in principle because the main theme is the implementation into the rotor simulation program. Nevertheless a short overview is necessary for this. So the value of a coefficient at any angle of attack is splitted up into a part belonging to the separated flow and a second part belonging to attached flow; see Fig. 5.

Separated flow is described by the Newtonian hypersonic flow law on the one side and by an additional term resulting from Rayleigh-Kirchhoff theory, combined with a new formulation of Kutta-condition that is described in detail in [14] and leads to a formulation of separated flow coefficients for all angles of attack. Here the first parameters have to be identified out of measurements; but the difficulty is that most measurements are not including angles of attack like 20° or 30° because of different reasons. Mostly wind tunnels are not able to have a correct measurement in those configurations on the one hand and on the other the profile will not act at such strange conditions later and therefore no one was interested to those data, but they are necessary for the validation of the model and for the adaption of the basic functions to special characteristics of the interesting profile.

The second and most important part is the description of attached flow that is superposed onto the separated flow model. This part consists of the formulation of several physical effects acting in this regime and it is splitted up into one formula belonging to the circulation of the upper side of the profile and another belonging to the lower side. Every circulation function consists of a normalized basic function with its maximum at the point of beginning stall. The value of the maximum is defined by a special function which strongly is depending on mach number like the point of beginning stall. The slope of the circulation function again is depending on mach number and is devided up into a subcritical and a transonic function so special transonic effects can be represented. To identify all parameters of these circulation functions a detailed set of steady profile measurements is necessary including positive and negative stall regime up to angles of attack where no more circulation exists and only separated flow represents the aerodynamic coefficients.

Identification of these parameters has been done by use of a least square method, optimising all parameters simultaneously [15]. Some results of an optimisation for the modified profile NACA 23012, that is used in the BO 105 rotor, are shown in Fig. 6. It is obvious, that the difference between measured and calculated data is very small at all mach numbers for lift, moment and even for drag.

In the case of sweep, that becomes very important at high advance ratios, already the steady profile behaviour changes in a special way. Here the point of beginning stall moves to greater values of angle of attack and so the maximum lift coefficient grows up to higher values than in the unswept case, as shown by experiments from Purser and Spearman, [16]. Although there are no measurements available under sweep conditions for the NACA 23012 profile, the principle behaviour must be the same as that of the NACA 0012 and so the additional parameters for representation of steady sweep are identified empirically. An Example is given in Fig. 7.

2.3.2 Unsteady aerodynamic coefficients

As mentioned before, a great advantage of the analytically formulation is the possibility to implement unsteady effects in a simple way. Mainly two effects have to be represented: the nonviscous circulation lag effect, that means the shift from the geometrical angle of attack to an effective one and the viscous boundary layer lag effect, that leads to a shifting of the stall angle. One principle assumption has been made: only harmonic motion is considered. This is a legal assumption in this case, because the simulation program is used for calculation of the wind tunnel model and this is working under steady conditions. The use of Duhamel-Integral in combination with the compressible Indicial function of Wagner [17] for harmonic oscillations in angle of attack and flap leads to an analytic expression for the lag of the angle of attack, depending on $\dot{\alpha}(t)$, $\ddot{\alpha}(t)$ of the profile, the coefficients of the Indicial functions (who are again a function of mach number) and on the frequency of the motion. Moreover noncirculatory flow effects like the apparent mass are represented by the model.

Some calculations with the set of parameters of the NACA 23012 profile are given in Fig. 8 for different conditions. Because there are no dynamic measurements for this profile available, measurement data are taken from the dynamic test of the NLR-1 profile [18]. Of course this profile has a different shape but in principle hysteresis loops should be similar. The main thing of these figures is the fact, that different frequencies at the same time can be calculated by this model in a very good way, because the measurement contained several higher harmonic amplitudes in angle of attack and these have been the input for the mathematical model, too.

Fig. 9 shows the effects of unsteady modelling on the effective angle of attack and on the effective stall angle for the case of Fig. 8. The solid line represents the angle of attack α and by addition of the dashed line, which is showing the $\Delta\alpha$ from circulation lag effects, the effective angle of attack is given. In most cases $\Delta\alpha$ is negative when $\dot{\alpha}$ is positive and vice versa, with a phase lag depending on mach number and frequency of oscillation. It is evident from this figure, that in most time steps the effective angle of attack is smaller than the geometrical one. On the other hand the shift of stall angle of attack, shown by the dashed-dotted line, is acting in the other way: the stall point is moving to greater angles when $\dot{\alpha}$ is positiv and vice versa but the phase shift is not so big as that of $\Delta\alpha$. Combination of both effects are leading to the hysteresis loop of Fig. 8.

Moreover there is an example of lift hysteresis under steady sweep condition in Fig. 10 showing the effects measured by Hilaire et al. [19]. Their result was that swept wing lift hysteresis loops are smaller than in the unswept case and in the same time they are reaching higher lift coefficients at the point of maximum lift. The reason is that stall onset begins at higher angle of attack and therefore a bigger part of the hysteresis lies within the linear region. Even this effect can be simulated in a perfect manner.

3 Implementation of unsteady aerodynamics into rotor simulation

At any radius of a rotor blade velocities are resulting from three effects. Firstly, the velocitiy of the free airstream is producing components normal and tangential to the rotor disc and therefore, depending on blade azimuth, a radial velocity leads to local sweep. Secondly, the velocities from blade motion have to be calculated. They are produced by rotation of the blade and the local velocities of the blade elastic

modes in flap and lag. The third component is the induced velocity, here described by the earlier mentioned method of Mangler or Beddoes and here only the normal component is used. All these velocities are superpositioned and transformed into the local profile coordinate system. For this transformation the local flapping angle $\beta(x,t)$, local lagging angle $\zeta(x,t)$ and the resulting local twist angle $\vartheta(x,t)$ must be known. They are approximately the gradients of the mode shapes and, in case of twist, the superposition of the control angles (ϑ_{07}, ϑ_S, ϑ_C and higher harmonics of them), the geometrical twist ϑ_T and the elastic torsion. After this, the velocities normal, tangential and radial to the local profile axis are known (V_z, V_x, V_r) and the angle of attack α is simple defined by tangential and normal velocity.

$$\sin\beta(x,t)\approx\beta(x,t)\approx\sum_{j=1}^{N_z}\frac{\partial\Phi_{zj}(x)}{\partial x}\cdot q_{zj}(t) \qquad \sin\zeta(x,t)\approx\zeta(x,t)\approx\sum_{j=1}^{N_y}\frac{\partial\Phi_{yj}(x)}{\partial x}\cdot q_{yj}(t)$$

$$\vartheta(x,t)=\vartheta_{07}+\vartheta_T\cdot(r/R-0.7)+\sum_l[\vartheta_{Sl}\cdot\sin(i\omega t)+\vartheta_{Cl}\cdot\cos(i\omega t)]+\vartheta_{el}(x,t) \qquad \alpha=arc\tan\frac{V_z}{V_x}$$

For one radial station the time history of angle of attack can be stored and analysed during the simulation using recursive harmonic analysis, where the rotor drive frequency is the basic frequency. By this procedure described in detail in [20] the amplitudes and phases of angle of attack oscillations at one radial station are identified during simulation and so they are available for the unsteady aerodynamic model. So, for the local unsteady aerodynamic coefficients, all data are present: angle of attack, its derivatives $\dot{\alpha}$ and $\ddot{\alpha}$ from the identified Fourier series, local mach number and, depending on this, the coefficients of Wagners step function.

Now the unsteady aerodynamic coefficients can be calculated and they lead to the unsteady load distribution along the blade in lift, drag and moment.

4 Results from unsteady rotor simulation

Calculations are made at advance ratios from $\mu = 0.0$ up to $\mu = 0.35$ to show the effects of this unsteady formulation on the local angle of attack. Thrust coefficient is held constant on the value of 0.0056 and the moments of the rotor are trimmed to zero. Variations are made in the downwash modelling (Mangler and Beddoes) and in the aerodynamic modelling (steady and unsteady) while the blade elastics are consisting out of three flapwise bending modes, two chordwise and one torsional mode in every case as mentioned before. During simulation the rotor was trimmed to match the required thrust and the moments becoming zero by variation of the three control angles for a given set of shaft angle and tunnel speed.

4.1 Hover condition

Hovering flight is an ideal condition to proof the unsteady calculation code because at any radial position the mach number is nearly constant for every azimuth and the trimmed rotor has no blade motion. So velocities and angle of attack are of steady nature and higher harmonic control in principle is the same as a forced angle of attack variation in wind tunnel except the degrees of freedom of the blades in flap, lag and torsion. Here variations are made from 1/rev up to 5/rev control with 2° amplitude and additional all together with 0.5° amplitude for every harmonic. Both variations are made with steady and unsteady aerodynamic modelling.

In Fig. 11 for the two radial positions of $r/R = 0.31$ and $r/R = 0.87$ the calculated amplitudes of the geometrical angle of attack α and its phase with respect to control phase, the effective angle of attack α_{eff} and its phase lag with respect to α are plotted. α is the result from all velocities acting at the given radius (including blade motion) and α_{eff} includes the $\Delta\alpha$ from Wagner function. It can be seen that for every radial station unsteady modelling leads to smaller amplitudes in α_{eff} in comparison to the geometrical angle of attack α although this one has the greater amplitude in the unsteady case. The reason is the counterphase of $\Delta\alpha$ reducing α. It should be noted that in the 1/rev case α-amplitude is reduced by the first flapping motion and therefore smaller than the control amplitude.

In principle a validation can be made at the radial position of $r/R = 0.87$ because here the mach number has the value of 0.56 and at 1/rev the frequency is $17.5Hz$ and therefore it is nearly the same condition as that of Fig. 9. There the 1/rev phase between α and α_{eff} is about 18° and in Fig. 11 a phase shift of about 14° can be seen so the results are very confidential in this case.

Of very special interest is the case of 3/rev, 4/rev and 5/rev control because these are the ones that can reduce vibration in forward flight. At 3/rev and at 4/rev an amplification of α_{eff} up to 5° at $r/R = 0.87$ is resulting from the low torsional eigenfrequency of about 3.7/rev and therefore we get an inphase torsional motion of the blade at frequencies below 3.7/rev and a counterphase motion at frequencies above. So at 4/rev at the inner position the amplitude of α_{eff} is reduced while at 3/rev it is still amplified. At 5/rev the amplitude of α_{eff} is very small because the circulation lag $\Delta\alpha$ is nearly as big as α itself and so the

effective amplitude is much smaller. In principle this effect occurs at all frequencies but the magnitude grows with the frequency of oscillation.

In Fig. 12 the blade mode reactions are shown for steady and unsteady modelling. At every control frequency the coordinated blade response amplitude of the three flapping modes and the torsional one, each as blade tip deflection, are presented showing the effects of unsteady modelling. It is obvious that in nearly all cases blade motion is reduced by unsteady aerodynamics following the smaller amplitudes of α_{eff} of Fig. 11. On the whole there are no extraordinary effects of unsteady modelling to be seen in comparison to steady aerodynamics except a small decrease of amplitudes in case of unsteady aerodynamics combined with a phase shift to higher azimuth of the rotor caused by circulation lag. An example for this global effect is shown in Fig. 13 where all higher harmonic controls from 1/rev up to 5/rev are set to a value of 0.5° simultaneously. The dotted curve represents the α from steady and the solid line the α from unsteady calculation while the thin solid line gives α_{eff}. In the outer region it can be seen very good that unsteady α has greater amplitudes than the steady one but the effective unsteady angle of attack again is smaller than the steady one. Additionally the phase shift of α_{eff} is evident. So it must be expected that unsteady calculation will give a smaller vibrational level than the steady aerodynamics when the profile is acting in the linear region like in the given examples before.

4.2 Forward flight

4.2.1 Global effects

Fig. 14 shows the shaft angle and the control angles for the four different model combinations over the total range of μ. It can be seen that in every case the Mangler downwash leads to smaller control angles in ϑ_C in the region of high vibration ($\mu \approx 0.1$) while at greater advance ratios the differences are negligible. The reason for this behaviour is the strong blade/vortex interaction at lower speeds which are not represented in the Mangler downwash formulation. At high speed, where the vortices are no more close to the following blades, the Mangler description differs not much from the Beddoes model and therefore the control angles are nearly the same.

Unsteady aerodynamics are leading to higher collective, proportional to μ (about 0.5° at $\mu = 0.35$) and to a more negative ϑ_S (about 0.75° at $\mu = 0.35$). The greatest effect appears in ϑ_C, where differences are up to more than 1°. In hover and at low speeds the Mangler formulation leads to higher values of collective pitch than necessary by using the Beddoes model. Hover measurements have shown that ϑ_{07} should be between 9° and 10° for the given thrust coefficient and therefore the Beddoes model is giving too small downwash velocities in this region. One possible reason for this behaviour may be the number of revolutions inside the wake. In these calculations 5 revolutions are calculated and this may be too few in the slow speed case. On the other hand HHC measurements made in 1988 [20] indicate that in ϑ_C the Beddoes model gives the best results even in the slow speed region so that the distribution of downwash is better represented by Beddoes. Only the mean value at lower speed is not high enough.

It is obvious that the downwash description from Beddoes should also result to a higher vibratory level than that of Mangler because of the local effects of blade/vortex interaction. Taking the 4/rev-amplitudes from the rotor forces and moments as an indicator for vibration as mentioned in [1] the vibration level results from the quality criterion GF as follows:

$$GF = \left(Fx^2 + Fy^2 + Fz^2 + Mx^2 + My^2\right)\Big|_{4/rev}$$

The value of this GF is plotted in Fig. 14 for the different models. At every speed the Beddoes downwash leads to higher vibratory levels (steady or unsteady aerodynamics) than that of Mangler; especially at $\mu = 0.1$ where measurements have shown the strongest vibratory level. At this speed unsteady aerodynamic formulation reduces the vibratory level in comparison with the steady model as expected in chapter 4.1. This indicates that all profile locations are acting in the linear region of lift curve without coming into stall effects and therefore the local effective angle of attack mostly is reduced by circulation lag effects, leading to smaller values of lift like shown in the two-dimensional case of Fig. 9.

At an advance ratio level of about $\mu = 0.2 - 0.3$ vibrations are at a minimum and growing again at higher speeds. HHC measurements of 1986 and 1988 have shown the minimum of GF between $\mu = 0.2$ and $\mu = 0.25$ so in this case steady aerodynamics in combination with Beddoes downwash are leading to the best predictions and the unsteady formulation is not bad, too. Only Mangler downwash leads to a minimum location at higher advance ratios. Very interesting is the behaviour at high μ because with Beddoes downwash unsteady modelling leads to a smaller vibratory level than in the steady case and with Mangler downwash the behaviour is just in other way. Here more and more induced velocity effects are vanishing and mach number effects are growing. Additionally on the retreating side the region of separated and reverse flow is expanding and also leading to vibration. So Mangler downwash seems to lead to higher local angle of attack more in the vicinity of stall than Beddoes downwash does and therefore stall effects are beginning to influence calculation in this case as will be shown later.

4.2.2 Local effects

Although there are a lot of data to be looked at here only the local effects of the different models on the blade segment angle of attack are under consideration because the main subject of this work was in the field of unsteady aerodynamics. The notation of the figures is the same as in Fig. 13 and data are taken at a radial position of $r/R = 0.93$ where blade/vortex interaction phenomena are occuring in a significant way.

Mangler downwash is the basis of Fig. 15 that shows the variations of α at $\mu = 0.1$ in Fig. 15a, $\mu = 0.2$ in Fig. 15b and $\mu = 0.35$ in Fig. 15c; Beddoes downwash is the basis of Fig. 16 that is built up in analogy to Fig. 15. At first sight the strong blade/vortex effect can be seen in Fig. 16 at $\mu = 0.1$ and at azimuth angle of $\psi \approx 70°$ on the advancing side and at $\psi \approx 290°$ on the retreating side. In principle the same can be found in Fig. 15 but only in a weaker form and therefore vibrations cannot be predicted well by Mangler in this speed range. At high advance ratio the curvature of α becomes very similar for both of the downwash models because the vortices are travelling downstream so fast that no significant blade/vortex interaction can occur.

Having a look at the circulation lag ($\Delta\alpha$) and the effective angle of attack that is built up from

$$\alpha_{eff}(\psi) = \alpha(\psi) + \Delta\alpha(\psi)$$

it is significant that at most azimuth the amplitude of α is reduced by unsteady effects. This leads to a smoother time history of α_{eff} and therefore to a smaller value of vibration when the profile is acting in the linear range of lift. On the same time, boundary layer lag effects $\Delta\alpha_{Stall}$ are moving the stall point in the opposite direction that means when α is reduced by $\Delta\alpha$ the stall point is amplified by $\Delta\alpha_{Stall}$ and vice versa. This is just in analogy to the effects shown in Fig. 9 and appears by use of Mangler and Beddoes downwash model. But this effect is of minor interest when the effective angle of attack is far away from stall in the cases of $\mu = 0.1$ and $\mu = 0.2$. Only at $\mu = 0.35$ stall effects are beginning to influence the calculation in case of Mangler downwash because the effective angle of attack at the retreating side grows up to more than 10° and on the same time the stall point moves to lower values of α (Fig. 15c) as indicated by $\Delta\alpha_{Stall}$. Using the Beddoes model in this case (Fig. 16c) effective angle of attack stays below 10° and $\Delta\alpha_{Stall}$ is positive that means the profile is acting in the linear regime of lift and so vibration level is not so much influenced as in the case of Mangler downwash.

In comparison to calculation with steady aerodynamics (dotted line) the unsteady effective angle of attack has significantly smaller amplitudes in the case of blade/vortex interaction (Fig. 16a) and a phase shift of its amplitudes to a greater azimuth that is well to be seen in Fig. 15a to 15c especially between $\psi = 45° - 90°$ on the advancing side.

5 Conclusions

A rotor simulation program has been coupled with a new code for representation of unsteady aerodynamic coefficients and two higher order wake models. It is shown that unsteady aerodynamics are influencing the vibratory airloads strongly depending on the downwash model; a high vibration level and correct control angles at low speed will be calculated right only when blade/vortex interaction is under consideration. Comparison with measurements indicates that the unsteady formulation is a step into the right direction but in most cases when the rotor is working in the linear lift region unsteady stall effects must not considered and it will be sufficient to have circulation lag effects included.

At high speed where the retreating side comes more and more into stalled condition and at low speeds combined with high thrust unsteady stall effects must be represented.

Future calculations will show effects in the stalled regime of maximum thrust and effects using higher harmonic control in forward flight where a lot of measurements have been made with this rotor.

Bibliography

[1] G. Lehmann *Untersuchungen zur höherharmonischen Rotorblattsteuerung bei Hubschraubern* DFVLR-FB 87-36

[2] E. Krämer, J. Hertel, S. Wagner *Computation of subsonic and transonic Helicopter Rotor Flow using Euler Equations* 13th European Rotorcraft Forum, Arles, France, Sept. 1987, Paper No. 14

[3] T. S. Beddoes *Practical Computation of unsteady Lift* 8th European Rotorcraft Forum, Aix-en-Provence, France, Sept. 1982, Paper No. 2.3

[4] D. Petot *Progress in the semi-empirical Prediction of the aerodynamic Forces due to large Amplitude Oscillations of an Airfoil in attached or separated Flow* 9th European Rotorcraft Forum, Stresa, Italy, Sept. 1983

[5] S. T. Gangwani *Synthesized Airfoil data Method for Prediction of dynamic Stall and unsteady Airloads* 39th Annual Forum of the American Helicopter Society, St. Louis, USA, 1983

[6] U. Leiss, S. Wagner *Analytische Darstellung der stationären und instationären aerodynamischen Beiwerte moderner Hubschrauberrotoren* DGLR-Jahrestagung, Bonn-Bad Godesberg, Germany, 1985

[7] K. W. Mangler *Calculation of the induced Velocity of a Rotor* Rep. No. Aero.2247, RAE, Farnborough, Great Britain, Feb. 1948

[8] T. S. Beddoes *A Wake Model for high Resolution Airloads* International Conference on Rotorcraft Basic Research, Research Triangle Park, NC, USA, 1985

[9] D. B. Bliss, M. E. Teske, T. R. Quackenbush *Free Wake Calculations using curved Vortex Elements* International Conference on Rotorcraft Basic Research, Research Triangle Park, N. C., USA, Feb. 1985

[10] K. W. Mangler *Fourier Coefficients for the Downwash at a Helicopter Rotor* RAE-Tech. Note No. Aero.1958, RAE, FARNBOROUGH, Great Britain, May 1948

[11] W. Johnson *Helicopter Theory* Princeton University Press, USA, 1980

[12] M. P. Scully *Computation of Helicopter Rotor Wake Geometry and its influence on Rotor harmonic Airloads* ASRL TR 178-1, 1975

[13] U. Leiss *Unsteady sweep - a Key to Simulation of threedimensional Rotor Blade Airloads* 11th European Rotorcraft Forum, 1985

[14] U. Leiss *Semi-empirical Simulation of steady and unsteady Blade aerodynamic Loading* International Conference on Rotorcraft Basic Research, Research Triangle Park, NC, USA, 1985

[15] H. G. Jacob *Rechnergestützte Optimierung statischer und dynamischer Systeme* Springer Verlag, Berlin, Heidelberg, New York, 1982

[16] P. E. Purser, M. L. Spearman *Wind Tunnel Tests at low Speed of swept and yawed Wings having various Planforms* NACA TN 2445, 1951

[17] R. L. Bisplinghoff, H. Ashley, R. L. Halfman *Aeroelasticity* Addison-Wesley Publishing Company, Inc., Reading, Massachusetts, 1957

[18] L. U. Dadone *Two-dimensional Wind Tunnel Test of an oscillating Rotor Airfoil* NASA CR-2914, 1977

[19] A. O. St. Hilaire, F. O. Carta, M. R. Fink, W. D. Jepson *The Influence of Wing Sweep in the aerodynamic Loading of an oscillating NACA 0012 Airfoil* NASA CR-3092, 1979

[20] G. Lehmann, R. Kube *Automatic Vibration Reduction at a four bladed hingeless Model Rotor - a Wind Tunnel Demonstration* 14th European Rotorcraft Forum, Milano, Italy, Sep. 1988

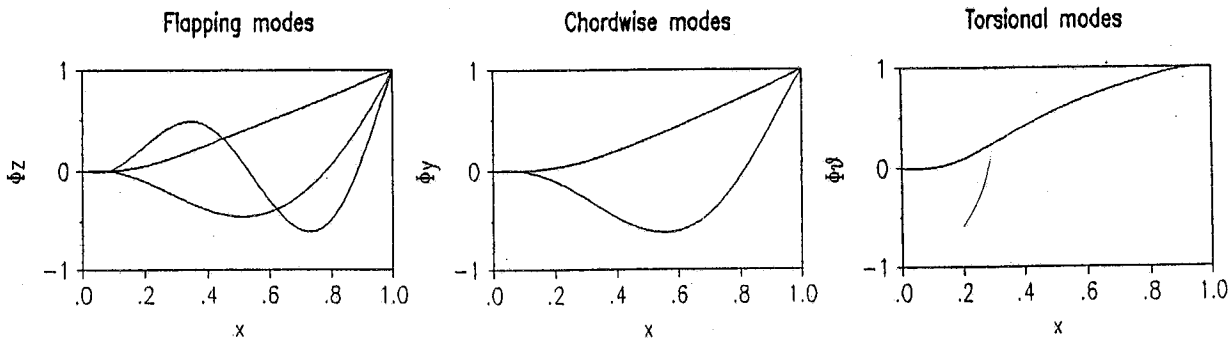

Figure 1. Modes of BO105 model rotor represented in simulation

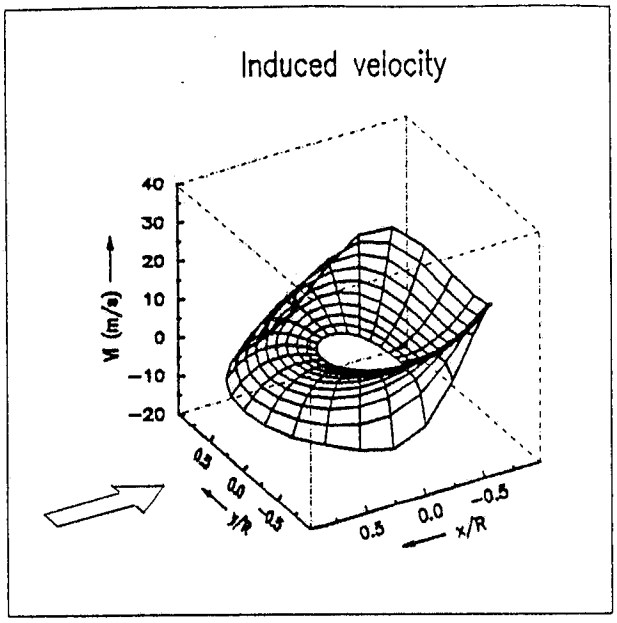

Figure 2. Downwash distribution (Mangler), $\mu = 0.15$, $C_T = 0.0056$

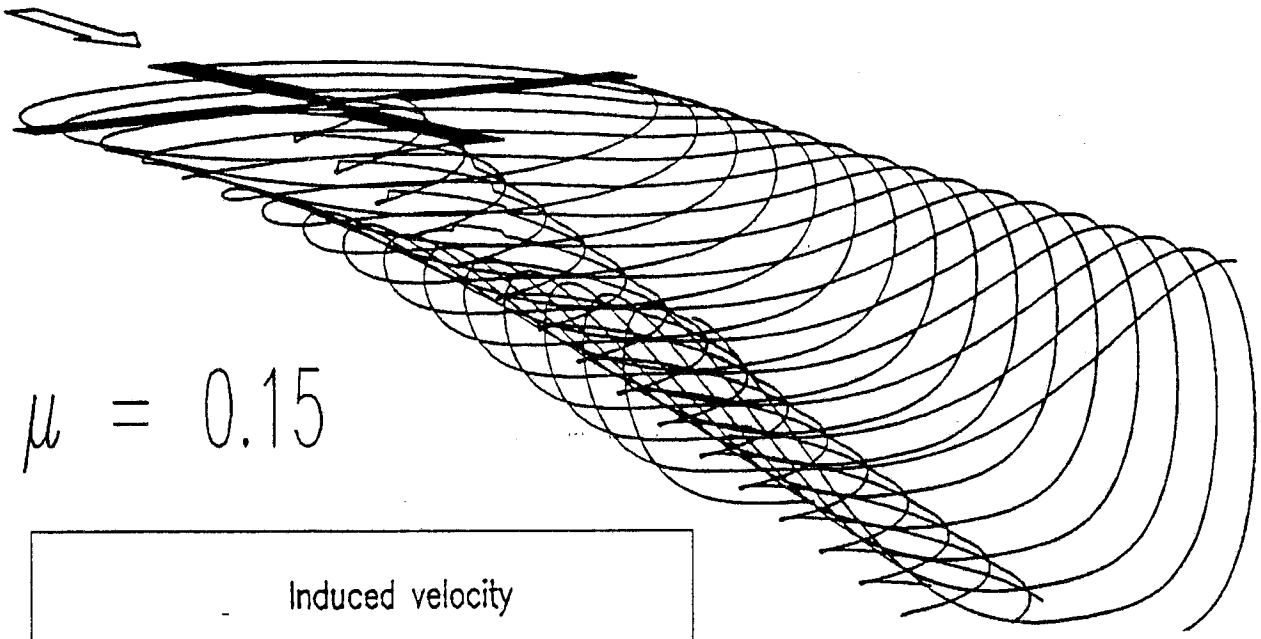

Figure 3. Vortex geometry of Beddoes downwash model, $C_T = 0.0056$, 4 revolutions, tip and root vortex plotted

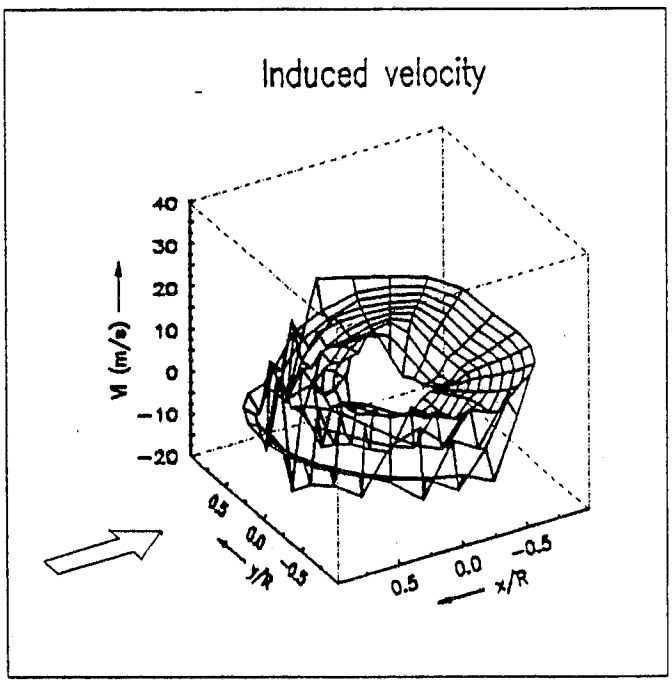

Figure 4. Downwash distribution (Beddoes), $\mu = 0.15$, $C_T = 0.0056$

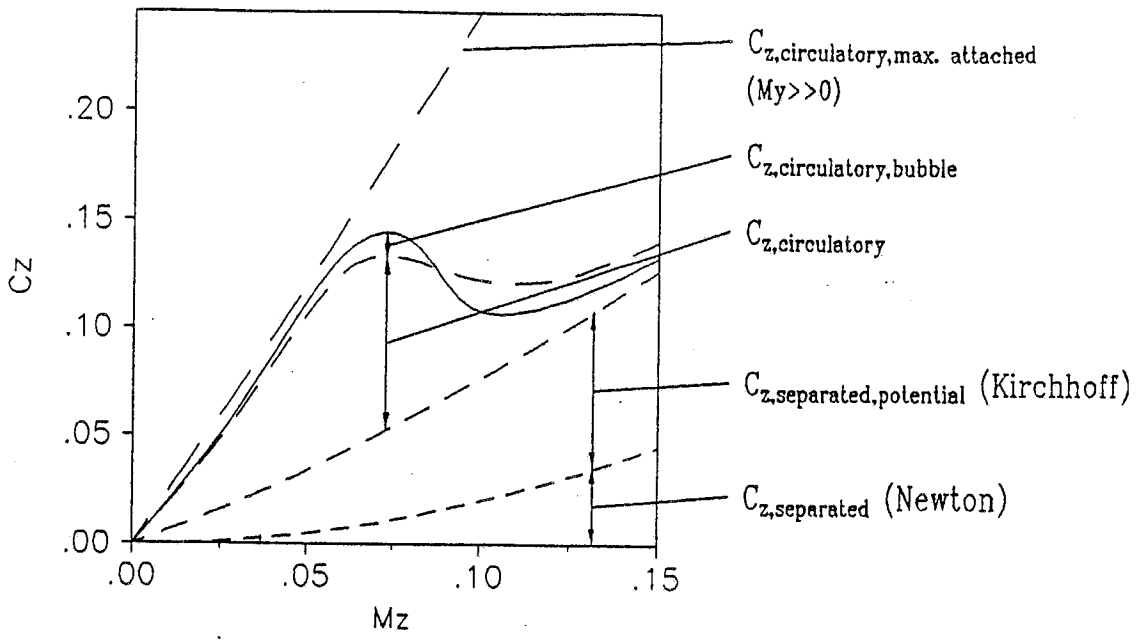

Figure 5. Principle structure of analytic coefficient modelling

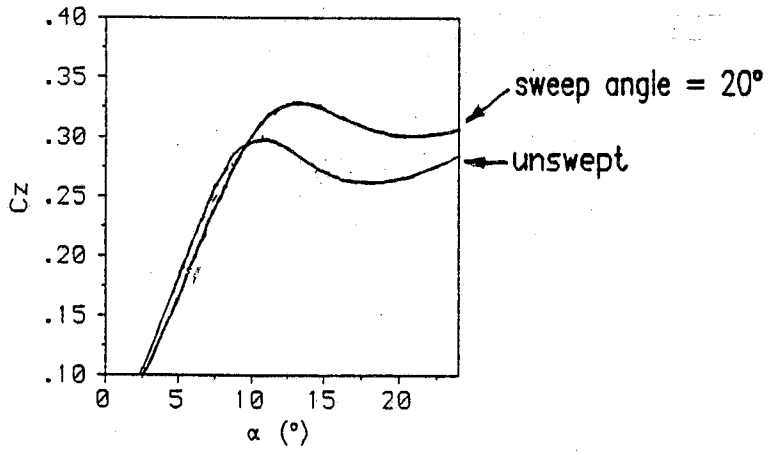

Figure 7. Influence of steady sweep, sweep angle $\varphi = 20°$, $M = 0.5$

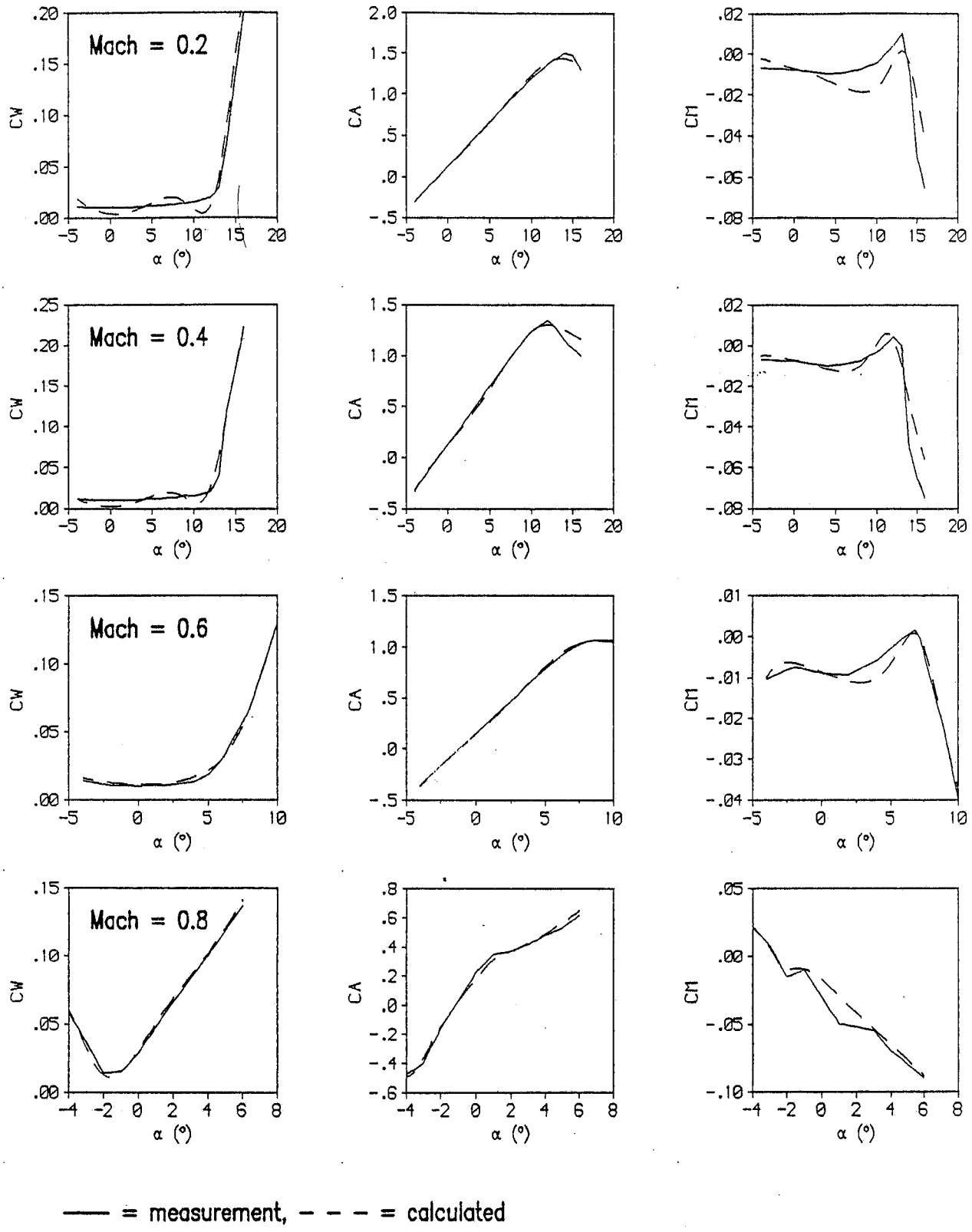

Figure 6. Comparison of calculated coefficients with measurement at different mach numbers

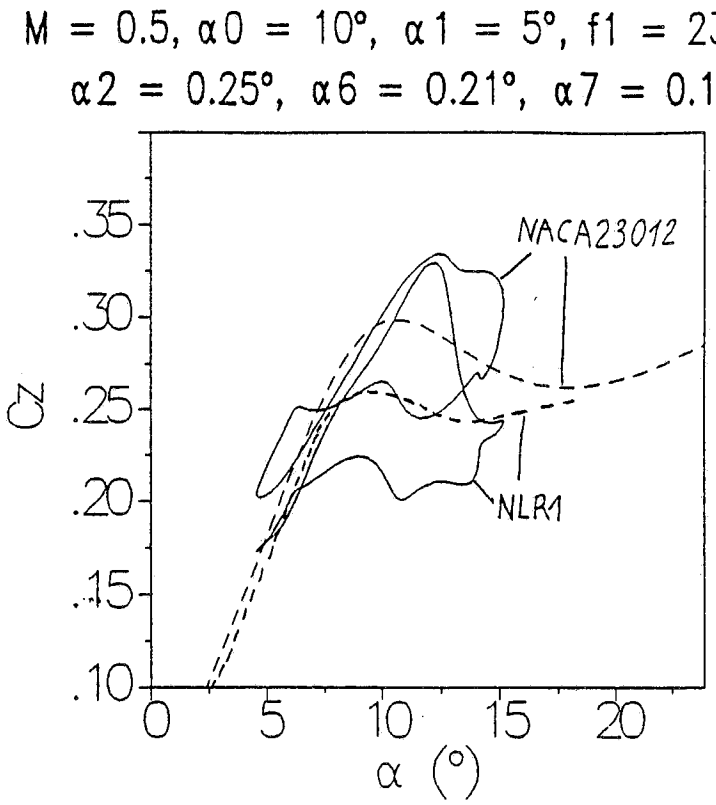

Figure 8. Lift hysteresis. Comparison of calculated NACA 23012 hysteresis with NLR1 measurement.

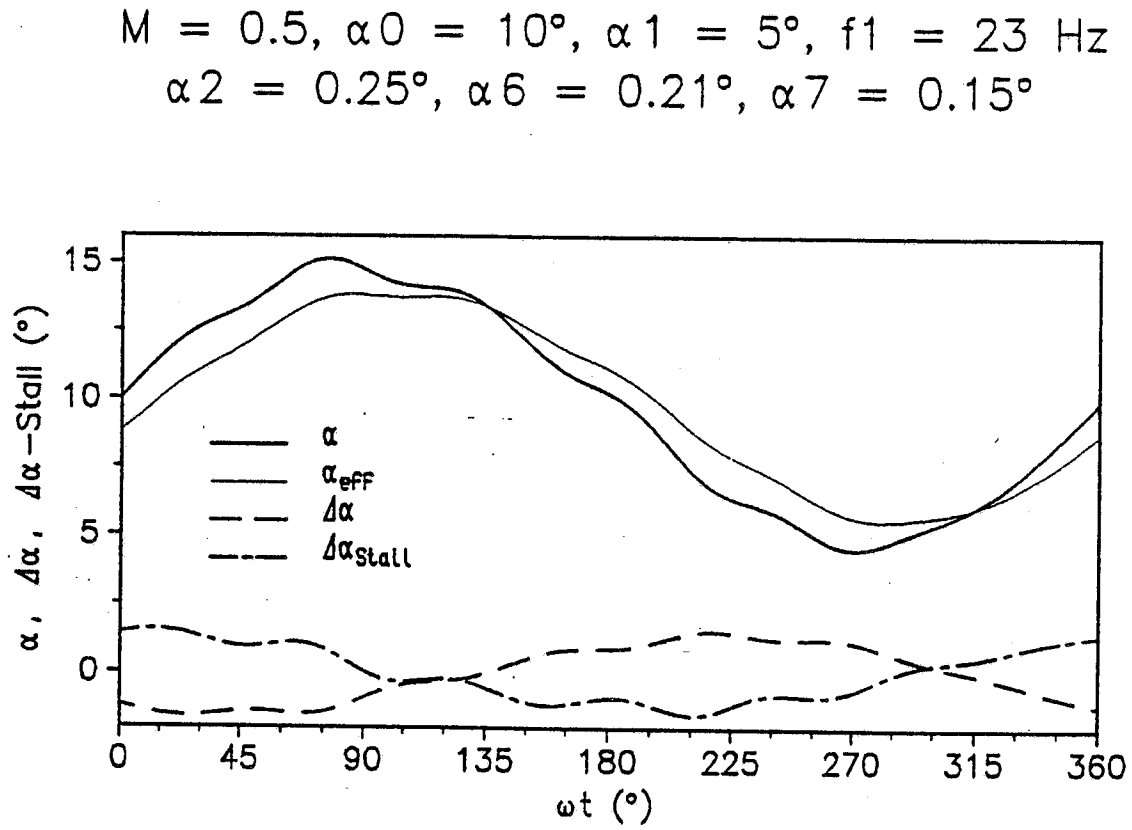

Figure 9. Unsteady effects in angle of attack α (moved by $\Delta\alpha$ to α_{eff}) and in stall angle (moved by $\Delta\alpha_{Stall}$)

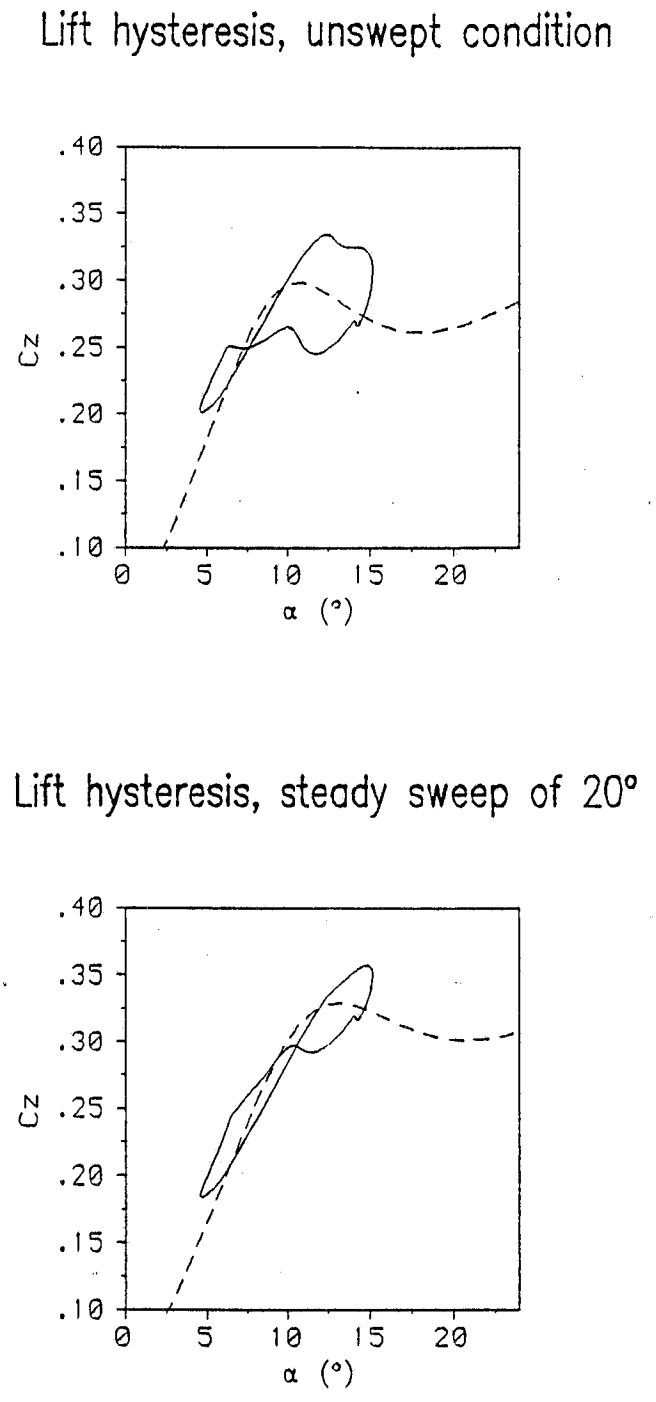

Figure 10. Unsteady lift hysteresis including steady sweep

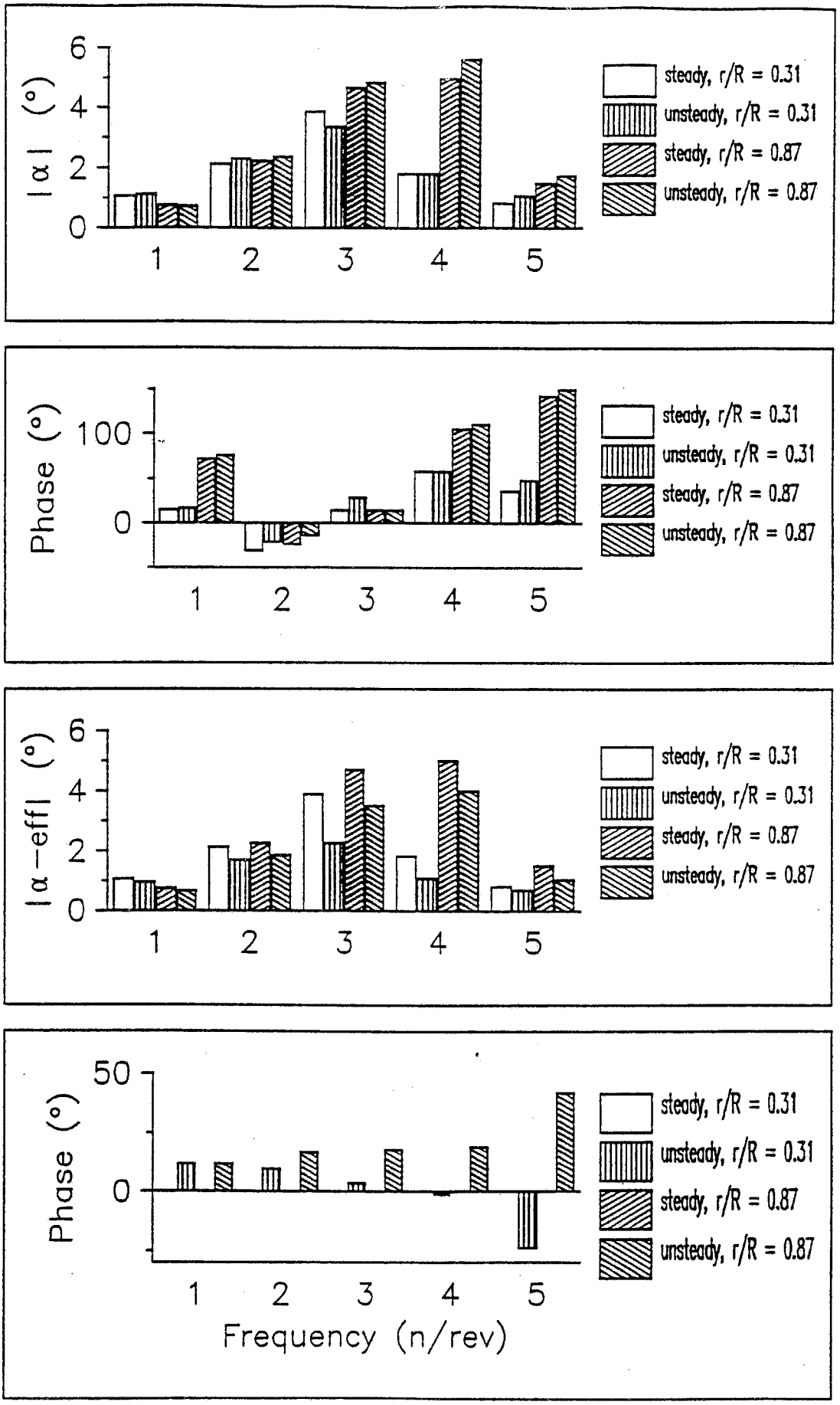

Figure 11. Unsteady effects on α at different radial stations and discrete higher harmonic control, $\mu = 0.0$, $C_T = 0.0056$, Mangler downwash

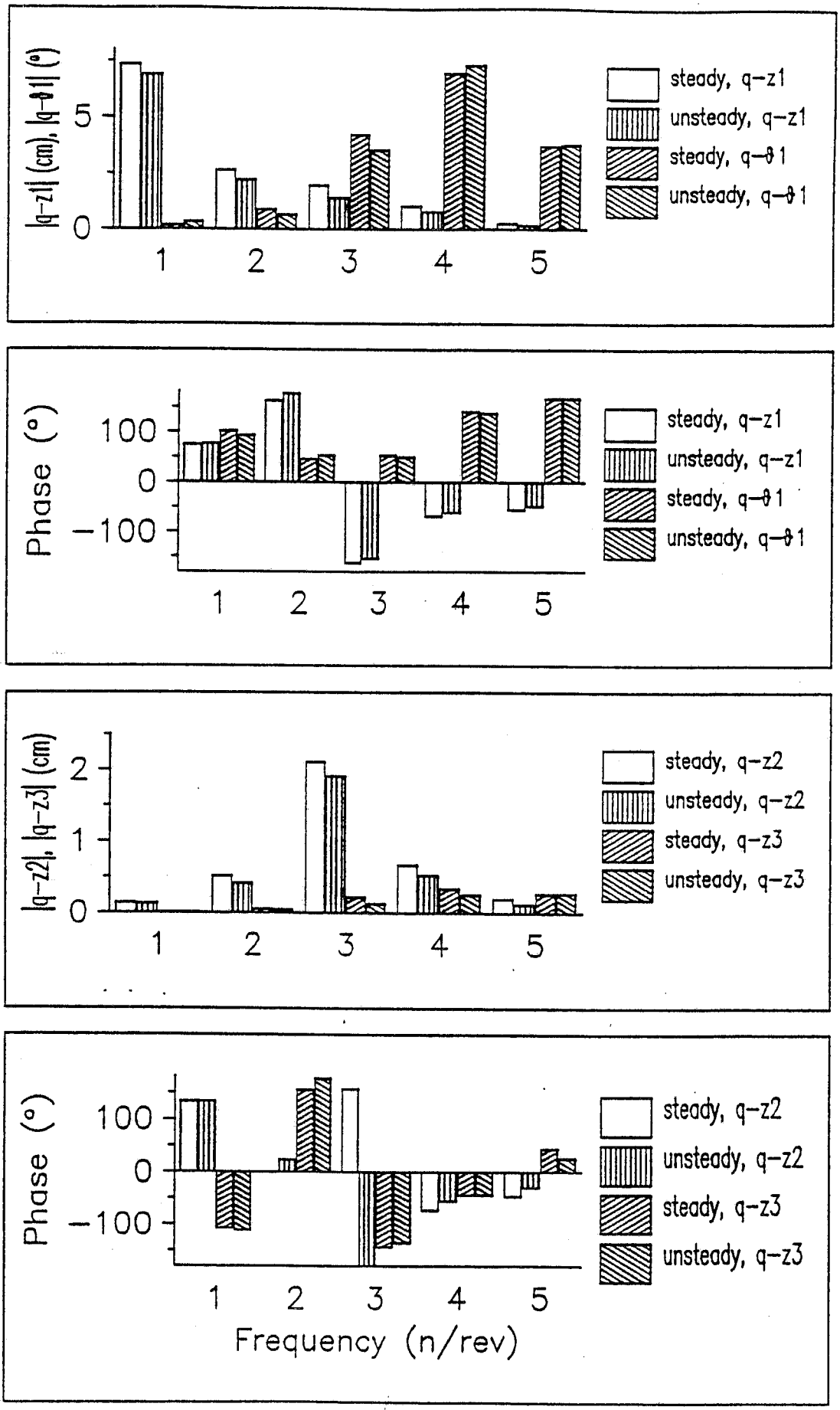

Figure 12. Unsteady effects on flapping and torsional motion at discrete higher harmonic control, $\mu = 0.0$, $C_T = 0.0056$, Mangler downwash

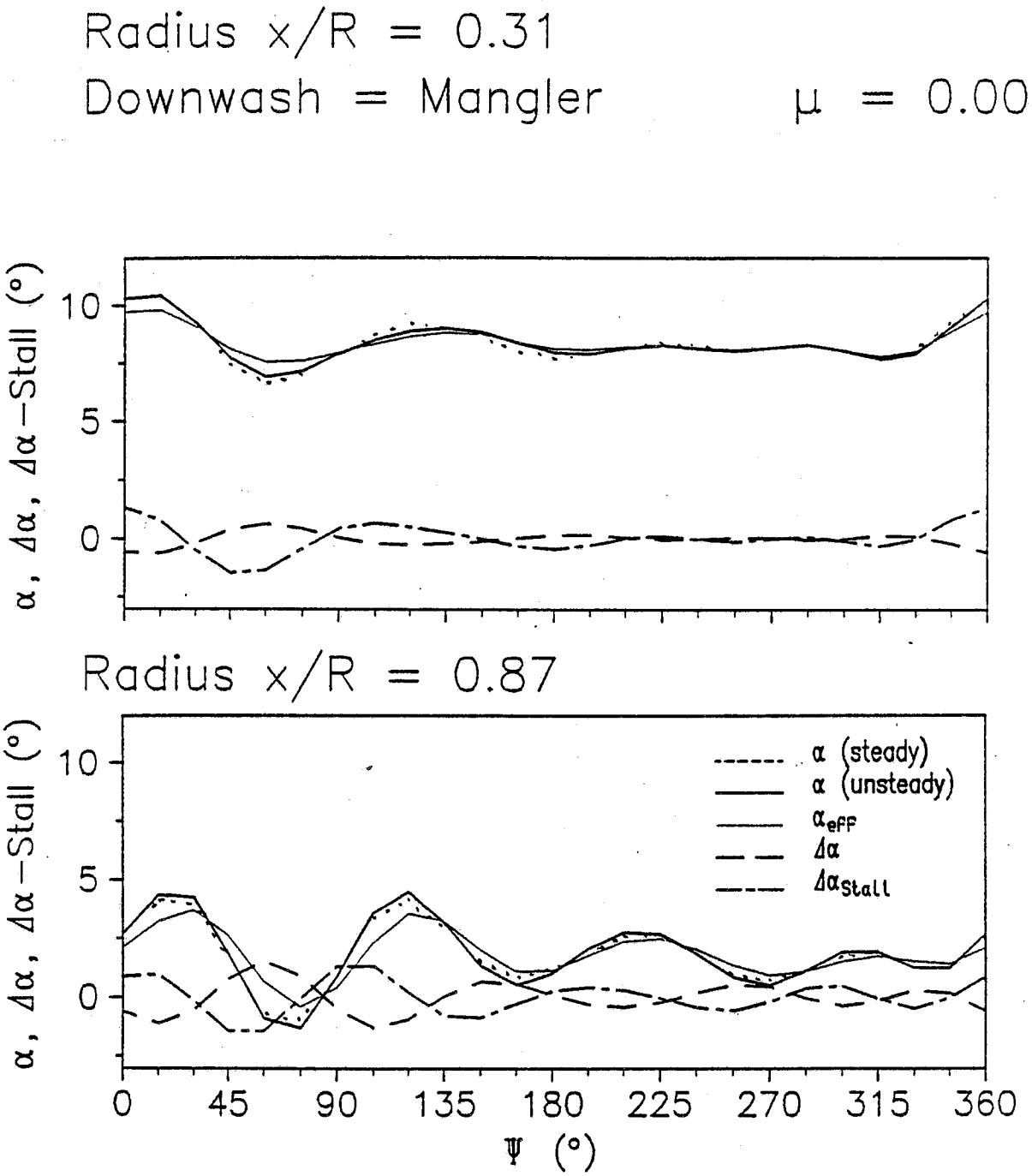

Figure 13. Unsteady effects on α at different radial stations by simultanouesly control of 1/rev up to 5/rev with 0.5° amplitude at each of them

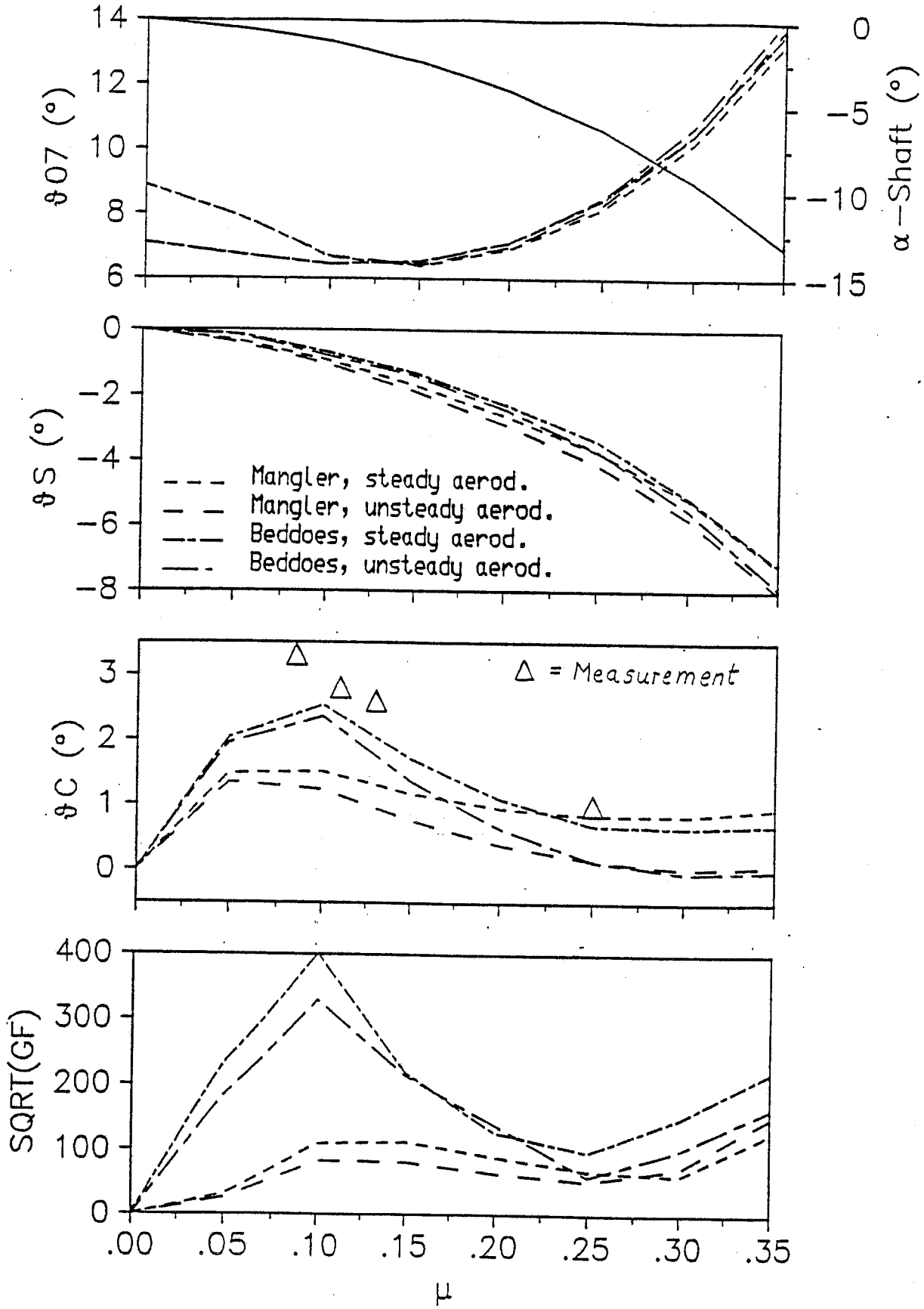

Figure 14. Shaft angle, control angles and vibratory level in forward flight with $C_T = 0.0056$ for steady and unsteady aerodynamic modelling and for different downwash models

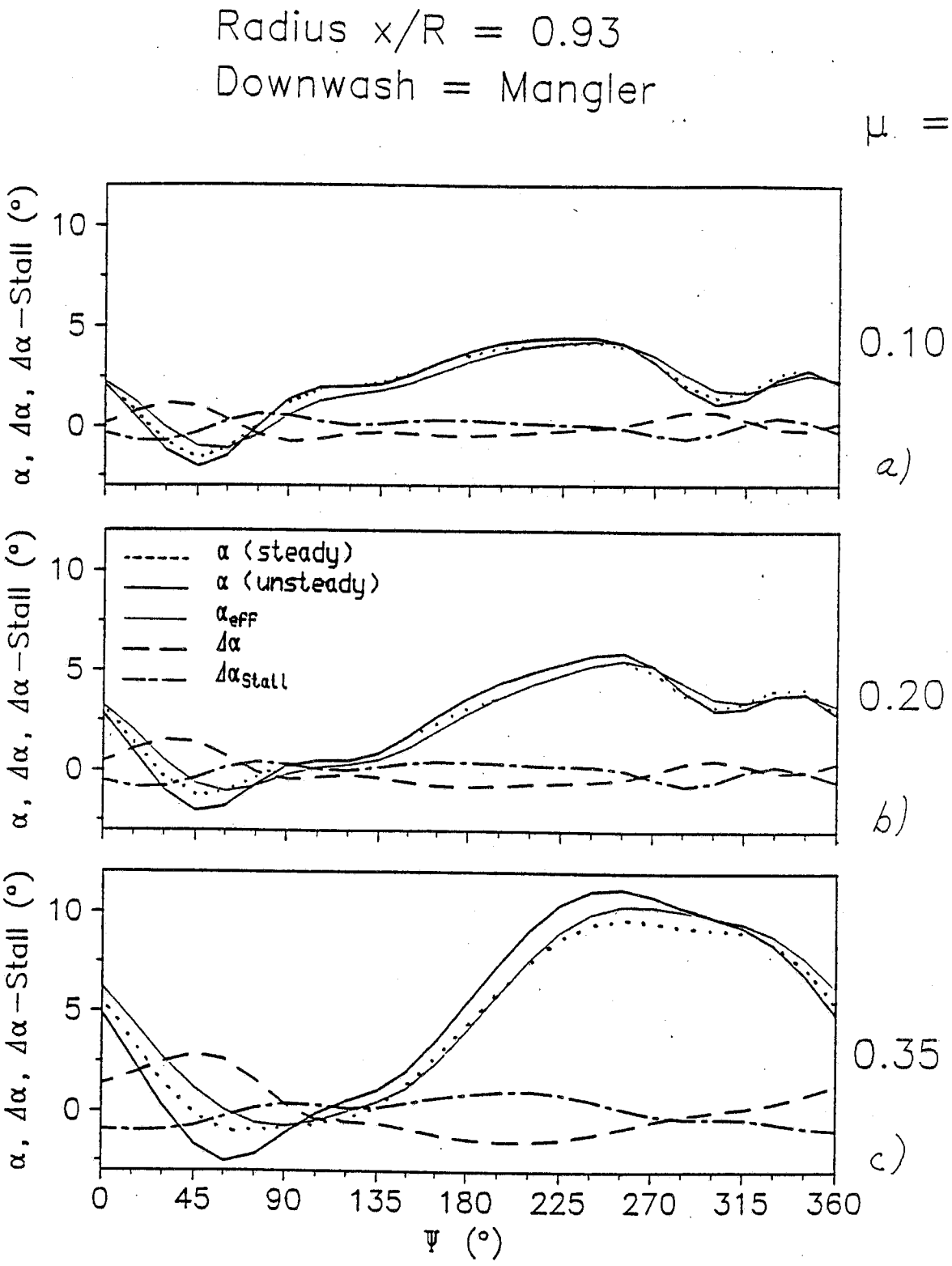

Figure 15. Unsteady effects on α and α_{Stall} at different advance ratios using Mangler downwash, $C_T = 0.0056$, $r/R = 0.93$

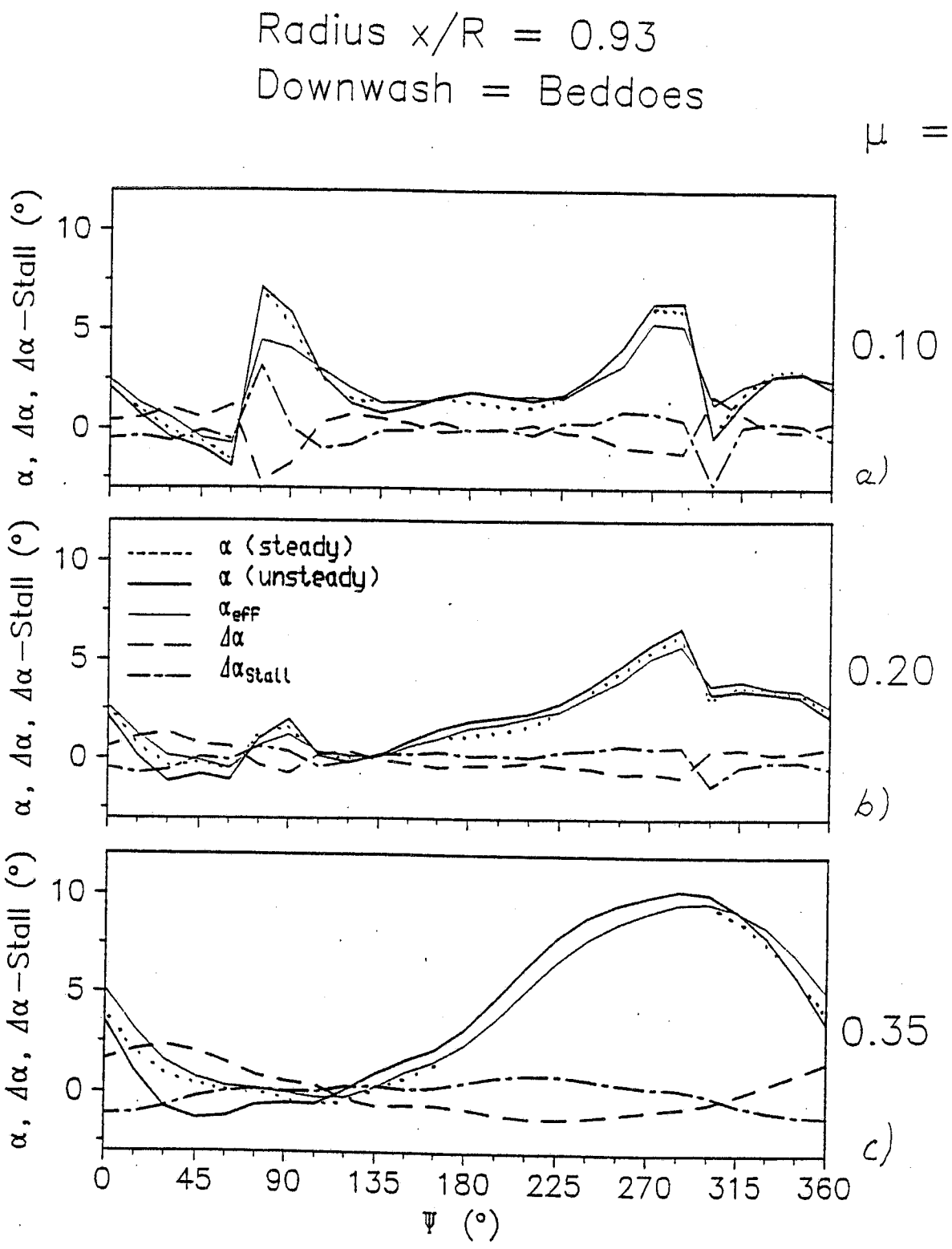

Figure 16. Unsteady effects on α and α_{Stall} at different advance ratios using Beddoes downwash, $C_T = 0.0056$, $r/R = 0.93$